Sustainable Calcination of Magnesium Hydroxide for Magnesium Oxychloride Cement Production

Gediminas Kastiukas, Ph.D.[1]; Xiangming Zhou, Ph.D., M.ASCE[2]; Babar Neyazi[3]; and Kai Tai Wan, Ph.D.[4]

Abstract: Effects of varying calcination conditions on the chemical and physical properties of magnesium oxide (MgO), an essential component of magnesium-based cement, were investigated using the more sustainable precursor material of magnesium hydroxide [$Mg(OH)_2$]. Extremely pure and thus more reactive MgO was obtained using a 17.6% less-energy-intensive calcination regime compared with industrial-grade MgO obtained from the calcination of dolomitic lime. As a result, the magnesium oxychloride cement (MOC) that was produced from the sustainably sourced MgO obtained a 50% increase in flexural strength and 22% increase in compressive strength. This was mostly due to its homogenous microstructure, consisting predominantly of the phase-5 hydration product, verified visually using a scanning electron microscope (SEM) and crystallographically using X-ray diffraction (XRD). Based on these findings, it has been revealed that the calcination therapies currently used in industry are impractical for both economic and sustainability purposes; MgO can be manufactured in a more sustainable and thus more competitive means, as discovered in this study. **DOI: 10.1061/(ASCE)MT.1943-5533.0002786.**

Introduction

Magnesia (MgO) has long been an important industrial material. As is well known, it is utilized in many industries ranging from refractory applications (Sako et al. 2012), in agriculture as a plant nutrient (Antonini et al. 2012), to wastewater treatment as an alkaline source to remove heavy metals (Purwajanti et al. 2015). It is also utilized in the manufacture of rubber and plastics, as well as in flue gas desulfurization for air pollution control (Gu et al. 2010; Marković et al. 2013; Yan et al. 2014).

MgO also has a 150-year history of being used in the form of calcined magnesium carbonate ($MgCO_3$) as a component in magnesium-based cement (Walling and Provis 2016). Magnesia-based cement, by definition, uses MgO as a building block rather than the CaO that comprises more than 60% of the elemental composition of portland cement (PC). This cement type is known by many different names, such as sorel, magnesite, and magnesium oxychloride (MOC) cement. There are two other known magnesia cements; the first is magnesium oxysulfate (MOS), which is the sulfate equivalent of MOC and is formed by the reaction between MgO and a magnesium sulfate solution (Chengyou et al. 2016). The second is magnesium phosphate cement (MAP), formed by the reaction between MgO and a soluble phosphate, such as dibasic ammonium phosphate ($NH_4H_2PO_4$) (Li et al. 2014).

MOC has many properties that are superior to those of PC. It does not need wet curing, has high fire resistance, low thermal conductivity, and good resistance to abrasion (Chau and Li 2008a; Li et al. 2013; Lu et al. 2015). It can also reach high compressive strengths of up to 85 MPa (Misra and Mathur 2007). MOC also bonds very well to a wide variety of inorganic and organic aggregates, such as sawdust, sand, and gravel (Li and Chau 2007; Zhou and Li 2012). The major commercial applications of MOC are industrial and residential flooring and decking (Li and Yu 2010), fire-protection coatings (Sglavo et al. 2011), and paneling (Chau and Li 2008a). Also, because of its resemblance to marble, it is used for rendering wall insulation panels and for stuccos (Chau and Li 2008b).

The main bonding phases found in hardened cement pastes are $Mg(OH)_2$, $5Mg(OH)_2 \cdot MgCl_2 \cdot 8H_2O$ (phase-5), and $3Mg(OH)_2 \cdot MgCl_2 \cdot 8H_2O$ (phase-3). The phase-5 is the phase with superior mechanical properties and can be formed using a molar ratio of $MgO:MgCl_2:H_2O = 13:1:12$ (Li and Chau 2007). The reactivity, i.e., overall MgO content, purity, and physical properties such as specific surface area (SSA), are the primary factors that will dictate the phase formation and thus final MOC material quality (Li and Chau 2008).

The magnesium-based cement industry predominantly relies on the use of dolomitic lime as a precursor source of MgO (Liu et al. 2015). However, deposits of dolomitic lime contain appreciable amounts of impurities, which are economically difficult to reduce (Sadik et al. 2018). The MgO formed from these minerals may contain from 5% to 20% of Fe_2O_3, Al_2O_3, and CaO in varying proportions. In addition, the typical calcination temperatures to produce light-burn MgO in industry are in the range of 900°C–1,050°C, and again, depend on the amount of impurities present (Seeley 2000).

Based on an exhaustive review of the most-cited MOC literature, all studies were found to use commercial-grade or in-house-prepared MgO derived from magnesite, i.e., $MgCO_3$.

[1]Research Fellow, Dept. of Civil and Environmental Engineering, Brunel Univ. London, Uxbridge, Middlesex UB8 3PH, UK. Email: Gediminas.Kastiukas@brunel.ac.uk

[2]Professor, Dept. of Civil and Environmental Engineering, Brunel Univ. London, Uxbridge, Middlesex UB8 3PH, UK (corresponding author). ORCID: https://orcid.org/0000-0002-6148-995X. Email: Xiangming.Zhou@brunel.ac.uk

[3]Graduate Student, Dept. of Civil and Environmental Engineering, Brunel Univ. London, Uxbridge, Middlesex UB8 3PH, UK. ORCID: https://orcid.org/0000-0001-7347-3261. Email: 1414667@brunel.ac.uk

[4]Lecturer, Dept. of Civil and Environmental Engineering, Brunel Univ. London, Uxbridge, Middlesex UB8 3PH, UK. Email: KaiTai.Wan@brunel.ac.uk

Note. This manuscript was submitted on June 25, 2018; approved on February 4, 2019; published online on April 27, 2019. Discussion period open until September 27, 2019; separate discussions must be submitted for individual papers. This paper is part of the ***Journal of Materials in Civil Engineering***, © ASCE, ISSN 0899-1561.

Furthermore, in cases where MgO was calcined in-house, details of calcination conditions were often omitted (Chau et al. 2009; Li and Chau 2007; Misra and Mathur 2007).

An alternative source of MgO proposed in this study is magnesium hydroxide [$Mg(OH)_2$], which can be derived relatively simply from magnesium-rich brine or seawater (Loganathan et al. 2017). $Mg(OH)_2$ can be considered as a more attractive option because its thermal decomposition does not release CO_2, only water vapor, and also offsets the problems associated with the depletion of high-grade ores through land-based mining. As of yet, there has been no reports on the synthesis of MgO at lower temperatures from $Mg(OH)_2$ for use as a precursor for the production of MOC. Thus, a better understanding of the relationships that exist between chemical and physical properties of MgO and such characteristics as calcination temperature and duration of $Mg(OH)_2$ would be highly desirable. Also, examinations of strength development, X-ray diffraction (XRD), and scanning electron microscopic (SEM) images of the reaction products presented in this study can be used as indices in the selection of proper molar ratios for obtaining optimal MOC cement from $Mg(OH)_2$-derived MgO.

Materials and Experiment

Materials

The $Mg(OH)_2$ and $MgCO_3$ precursors (<5% impurities), a commercial MgO powder derived from calcined dolomite used as a commercial reference, and magnesium chloride hexahydrate crystals ($MgCl_2 \cdot 6H_2O$) of 98% purity were all obtained from Magnesia, Lüneburg, Germany. The chemical characteristics of the $MgCO_3$, $Mg(OH)_2$, and commercial magnesium oxide (C-MgO) were analyzed by wavelength dispersive X-ray fluorescence (WD-XRF) spectrometry (Axios mAX, Malvern Panalytical, Worcestershire, UK), and are listed in Table 1. The following abbreviations are used to denote the different MgO powders: MgC for MgO derived from $MgCO_3$; MgH for MgO derived from $Mg(OH)_2$; and C-MgO for the reference commercial MgO. In addition, the calcination temperature and calcination duration were added to the latter abbreviations. For example, MgH-650/1 refers to MgO from the calcination of $Mg(OH)_2$ at 650°C for 1 h.

Precursor Powder Calcination

The preparation of MgO was based on the calcination of $Mg(OH)_2$ $MgCO_3$ precursor powders under a range of calcination temperature and calcination time combinations. In a typical synthesis, 50.00 ± 0.005 g of precursor powder was weighed into a ceramic crucible, transferred to a 3-L-capacity furnace operating under static air (Carbolite, Hope, UK) and calcined at temperatures of 650°C or 850°C for either 1 or 2 h at a ramp rate of 20°C/min.

Table 1. Chemical composition of the magnesium carbonate ($MgCO_3$), magnesium hydroxide [$Mg(OH)_2$], and commercial magnesium oxide (C-MgO)

Component	$MgCO_3$ (%)	$Mg(OH)_2$ (%)	C-MgO (%)
MgO	45.46	68.6	95.44
CaO	1.21	0.30	1.76
SiO_2	2.61	0.08	0.38
Fe_2O_3	0.08	0.023	0.03
Al_2O_3	0.04	0.05	0.01
LOI	50.1	30.5	2.32

Table 2. Calcination conditions of the precursor powders

Sample reference	Precursor type	Calcining temperature (°C)	Calcining time (h)
MgC-650/2	$MgCO_3$	650	2
MgH-650/2	$Mg(OH)_2$	650	2
MgC-850/2	$MgCO_3$	850	2
MgH-850/2	$Mg(OH)_2$	850	2
MgH-650/1	$Mg(OH)_2$	650	1
MgH-850/1	$Mg(OH)_2$	850	1

The calcination conditions of the $MgCO_3$ and $Mg(OH)_2$ are included in Table 2.

MOC Sample Preparation

The required amount of $MgCl_2 \cdot 6H_2O$ was first added in deionized water and, using a magnetic stirrer, dissolved until a clear solution was obtained. Selected samples of MgO based on chemical and physical properties were carried forward for the production of the MOC paste. Batches of typically 1.0 kg were prepared using a laboratory bench-top mixer by combining the $MgCl_2 \cdot 6H_2O$ solution and MgO powder for 5 min. $MgO/MgCl_2$ molar ratios of 3, 5, and 9, along with a constant $MgO/MgCl_2$ ratio of 10, were used in the preparation of all samples. The water to solids ratio (w/s) was initially fixed at 0.22 for all compositions studied. However, to achieve adequate and consistent paste rheology, the water content was altered as necessary. Following mixing, three prismatic $20 \times 20 \times 160$-mm specimens were cast for each sample, with vibration compaction being implemented to reduce the air-void content as much as practically possible. After casting, the specimens were air-cured for 7 days at a temperature of $25°C \pm 1°C$ and relative humidity of $60\% \pm 5\%$.

Test Procedures and Characterization

The $20 \times 20 \times 160$-mm specimens were utilized to conduct the three-point flexural testing first. Then, the broken remains were used for the compression testing. Both tests were carried out using a 50-kN universal testing machine (Instron 5960, High Wycombe, UK) at a loading rate of 12.7 mm/min. The XRD patterns of all samples were obtained using a Bruker D8-Advance X-ray diffractometer (Madison, Wisconsin) with Cu Kα radiation ($\lambda = 1.5418$ Å), with the operation voltage and current maintained at 40 kV and 40 mA, respectively. SEM images were obtained with a JEOL JSM-6330F (JOEL, Tokyo) operated at a beam energy of 20.0 kV. Particle-size analysis and specific surface area measurements were performed using a Mastersizer 2000 (Malvern Instruments, Worcestershire, UK). The rate at which MgO reacted with a dilute solution of acetic acid was used as a measure of its activity. An excess of MgO was used so that at the end of the reaction, the solution turned from acidic to basic and was detected by a color change employing a phenolphthalein indicator.

Results and Discussion

Calcination Performance

The major chemical compositions of the commercial MgO and the MgO obtained from calcination of $MgCO_3$ and $Mg(OH)_2$, analyzed by WD-XRF, are presented in Table 3. Chemical analysis of the commercial MgO (C-MgO) indicated a $96.21\% \pm 0.1\%$ MgO content, with calcium, silicon, iron, aluminum, and sulfur oxides appearing as the major impurities. Regarding the calcination

Table 3. Chemical compositions of commercial MgO and the MgO obtained from calcination of $MgCO_3$ and $Mg(OH)_2$

Sample reference	MgO	SiO_2	CaO	Al_2O_3	Fe_2O_3	Mn_3O_4	SO_3
C-MgO	96.21	0.35	1.81	<0.01	0.05	<0.01	0.01
MgC-650/2	90.18	6.475	2.59	0.13	0.49	<0.01	0.05
MgH-650/2	98.99	0.23	0.53	0.06	0.07	<0.01	0.14
MgC-850/2	91.48	5.48	2.54	0.06	0.17	<0.01	<0.01
MgH-850/2	98.91	0.20	0.61	0.09	0.06	<0.01	0.07
MgH-650/1	98.98	0.22	0.61	0.08	0.04	<0.01	0.07
MgH-850/1	98.60	0.21	0.67	0.14	0.10	0.05	0.10
MgH-850/6	99.0	0.22	0.56	0.08	0.03	<0.01	0.07

of $MgCO_3$ at the two different temperatures of 650°C and 850°C, i.e., samples MgC-650/2 and MgC-850/2, the quantity of MgO obtained was practically the same at 90.18% and 91.48%, respectively. The calcination temperature of $Mg(OH)_2$ did not induce any change in the content of MgO produced because calcination at 650°C and 850°C for 1 h resulted in 98.99% and 98.91% of MgO, respectively. Increasing the calcination time from 1 to 2 h for samples of $Mg(OH)_2$ calcined at 650°C or 850°C did not induce any significant change in the MgO content either, consistently remaining in the range of 98.60%–98.99%. What was apparent was the significant difference in MgO content between the calcined $MgCO_3$ and $Mg(OH)_2$. An increase of 8.8% in MgO content was measured for the $Mg(OH)_2$ calcined at 650°C for 2 h (MgH-650/2) compared with the $MgCO_3$ calcined at the same conditions, i.e., MgC-650/2.

Finally, a prolonged temperature hold of $Mg(OH)_2$ calcination did not affect the efficiency of $Mg(OH)_2$ transformation to MgO · $Mg(OH)_2$ calcined for 1 h (MgH-850/1) compared with $Mg(OH)_2$ calcined for 6 h (MgH-850/6) produced an almost identical MgO content, i.e., 98.6% and 99.0%, respectively. The latter proves that a calcination regime of 1 h is sufficient to produce a high MgO yield.

Further features revealing the calcination performance of $Mg(OH)_2$ compared with the commercial MgO are presented in Table 4. The results clearly indicate that the loss on ignition (LOI) measured for the calcined $Mg(OH)_2$ samples were at least 97% lower than that of the commercial MgO. The latter is indicative of the presence of carbonate in the commercial MgO due to incomplete combustion of the $MgCO_3$. It also confirms that the calcination conditions applied in the preparation of the MgO from $Mg(OH)_2$ investigated in this study were sufficient because LOI was measured to be <0.2%. It was also evident that the LOI decreased more so due to the increase in calcination temperature than calcination time. The specific surface of the MgH-650/1 was measured to be 35% higher than of the C-MgO, which gives an indication of the increased reactivity of the MgO produced in this study. The calcination time did not significantly affect the specific surface area and, thus, temperature remained as the primary process variable. The activity of the MgO increased with calcination temperature and thus, reactivity (inversely proportional to activity) decreased.

Table 4. Physical properties of commercial MgO and MgO obtained from $Mg(OH)_2$ calcination

		Calcination temperature and calcination time of $Mg(OH)_2$			
		1 h		2 h	
Property	C-MgO	650°C	850°C	650°C	850°C
Loss on ignition (%)	2.32	0.18	0.11	0.15	0.10
Specific surface area (m^2/g)	1.07	1.65	1.59	1.65	1.58
Activity (s)	17	11	26	12	35

The variation of reactivity with temperature correlates well with that observed for the measured specific surface area. The lowest activity value and the highest specific surface area, which indicates the most reactive MgO, was obtained through calcination at 650°C and 1 h. Previous studies related to examining calcinations conditions of $MgCO_3$ recommended a temperature of 900°C and time of 4 h (Birchal et al. 2001). Also, in the study of Zhu et al. (2013), MgO with the highest hydration conversion ratio was obtained with an activity of 40 s by calcinating $MgCO_3$ at 600°C for 1.5 h. However, this was accomplished with a trade-off for a very low decomposition ratio of $MgCO_3$.

The hypothesis that the calcination temperature is the more dominant influence in controlling the MgO content as opposed to the time of calcination is further supported by the XRD spectra presented in Fig. 1. It illustrates that $Mg(OH)_2$ calcined at 650°C for both 1 and 2 h durations exhibited almost equivalent peak characteristics, i.e., peak intensities and relative peak positions.

Furthermore, almost identical peak characteristics were found to exist between the commercial MgO (C-MgO) and MgO obtained from calcination of $Mg(OH)_2$ at 650°C for 1 h (MgH-650/1), as shown in Fig. 2. These findings provide beneficial implications for future practical usage purposes because they demonstrate that it is highly possible to use $Mg(OH)_2$ to produce a high quality (chemically pure) MgO comparable with that of commercial MgO.

Further XRD spectra presented in Fig. 3 of two samples of MgO obtained from $Mg(OH)_2$ and $MgCO_3$ via the same calcination

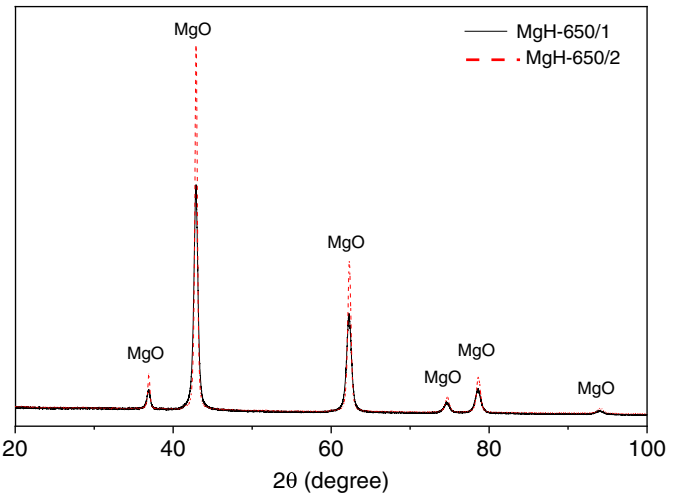

Fig. 1. XRD spectra of MgO obtained from calcination of $Mg(OH)_2$ at 650°C for 1 and 2 h.

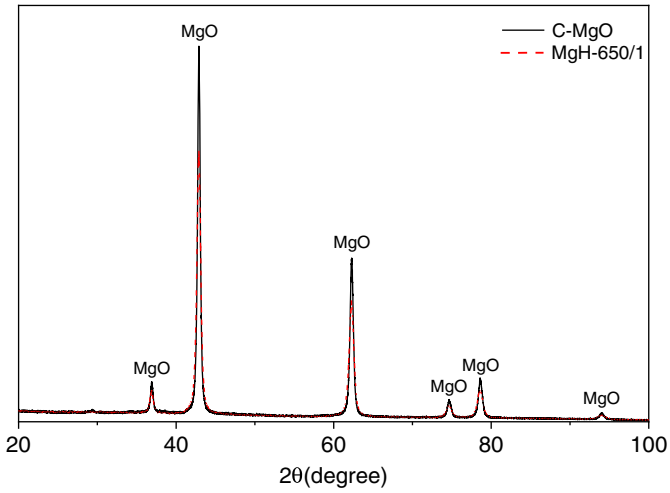

Fig. 2. XRD spectra of commercial MgO and MgO obtained from calcination of $Mg(OH)_2$ at 650°C for 1 h.

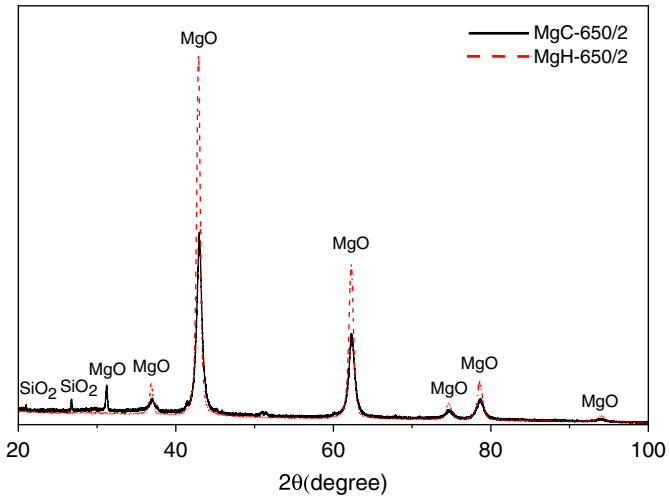

Fig. 3. XRD spectra of MgO obtained from calcination of $Mg(OH)_2$ and $MgCO_3$ at 650°C for 2 h.

conditions (calcination temperature and duration) illustrate a vast difference in the identified peak intensities of MgO, as well as a varied chemical composition. More specifically, the identified MgO peaks belonging to the MgO sample (MgH-650/2) obtained from $Mg(OH)_2$ have a significantly higher intensity than the MgO sample (MgC-650/2) obtained from $MgCO_3$. It is also observable that contamination is present in the chemical composition of the sample MgC-650/2 in the form of silicon dioxide (SiO_2), indicating its reduced purity.

Energy Requirements of $Mg(OH)_2$ *and* $MgCO_3$ *Calcination*

The energy requirements involved in the calcination of $Mg(OH)_2$ and $MgCO_3$ is another controlling factor in the production of MgO. During the calcination of $MgCO_3$, the decomposition reaction involves the undesirable emittance of CO_2, as expressed in the following thermal decomposition reaction:

$$MgCO_3 + \text{heat} \rightarrow MgO + CO_2 \quad (1)$$

At 650°C, 1 kg of $MgCO_3$ was found to yield 0.501 kg of MgO and 0.499 kg of CO_2. The latter calculation is based on the assumption that all MgO powders were dry before the calcination process, and residual water possibly adsorbed onto the magnesium oxide surfaces in a monolayer was ignored. Therefore, it can be calculated that for manufacturing purposes, 2.01 kg of $MgCO_3$ is required to produce just 1.00 kg of MgO.

In comparison, $Mg(OH)_2$ can be considered a much more energy-efficient precursor for obtaining MgO because it only emits H_2O, as expressed in the following thermal decomposition reaction:

$$Mg(OH)_2 \rightarrow MgO + H_2O \quad (2)$$

Also at 650°C, 1 kg of $Mg(OH)_2$ when fully decomposed yielded 0.685 kg of MgO and 0.315 kg of H_2O. More importantly, no CO_2 originating from decomposition was emitted during calcination.

The energy required to raise the temperature of the hydroxide solids from ambient temperature (298 K) to the decomposition temperature of 350°C (623 K) can be calculated using the specific heat capacity of magnesium hydroxide at 600 K (1.78 kJ/kg K) as follows:

$$1.78 \text{ kJ/kg K} \times 0.685 \text{ kg} \times 325 = 396 \text{ kJ} \quad (3)$$

Once the solids are at decomposition temperature, the energy required to effect the decomposition can be calculated from the enthalpy of decomposition, which at 600 K is 1,304 kJ/kg

$$1{,}304 \text{ kJ/kg} \times 0.685 \text{ kg} = 893 \text{ kJ} \quad (4)$$

The total energy required to decompose 1 kg $Mg(OH)_2$, which will lead to 0.685 kg of MgO and water vapor, is the sum of 893 + 396 = 1,289 kJ (1,221 Btu). The energy needed to be expended to produce 1 t of MgO will, therefore, be 1,881 MJ (1.78 MBtu).

Performing the same latter calculations for $MgCO_3$ using a specific heat capacity of 116.2 J/mol · K yields an energy requirement of 999 kJ/kg. The enthalpy of decomposition of $MgCO_3$ at 650°C is 1,284 kJ/kg, which is the energy required for the second step. This gives a total energy requirement of 999 + 1,284 = 2,283 kJ (2,163 Btu) to decompose 1.0 kg of $MgCO_3$, or 2.28×10^6 kJ per 1 t [2,283 MJ (2.16 MBtu)].

This proves that as well as the significant benefit of not emitting CO_2, the calcination process of $Mg(OH)_2$ is 17.6% less energy intensive than that of $MgCO_3$ and yields 26.8% more MgO.

Morphology of Calcined MgO

The morphological characteristics of the MgO samples Mg-H-650/1, Mg-H-850/1, and C-MgO were also observed using the electron microscope and are presented in Fig. 4. Fig. 4(a) of MgH-650/1 shows a largely balanced particle-size distribution with the mean particle size being measured as 6.54 μm. Most of the MgH-650/1 particles are distinctly separate from each other and did not agglomerate during calcination. Avoiding agglomeration would essentially provide for more contact area, thus leading to a higher rate of reaction. The morphology of sample MgH-850/1 seen in Fig. 4(b), however, is vastly different; MgH-850/1 particles have agglomerated due to a higher calcination temperature, resulting in an increased mean particle size of 8.056 μm. Moreover, it can be seen from Fig. 4(c) that the particle distribution of C-MgO is largely irregular, with particle sizes ranging from small (approximately 2–3 μm) to large (approximately 15 μm). Also, agglomeration of C-MgO particles is similar to that observed for MgH-850/1. As discussed previously, this would result in a larger mean

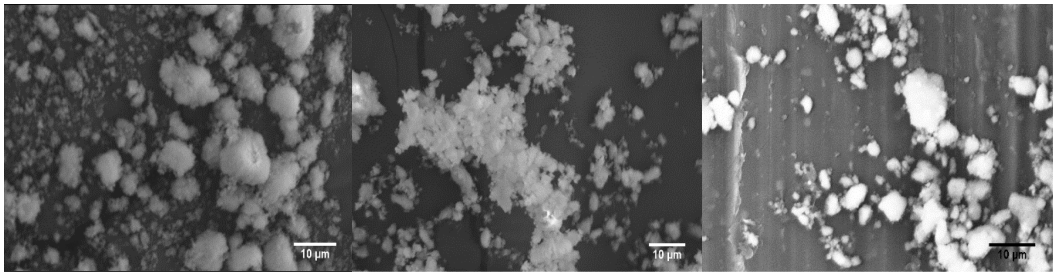

Fig. 4. Morphological characteristics of MgO samples: (a) MgH-650/1; (b) MgH-850/1; and (c) C-MgO.

particle size and lower surface area because sample C-MgO had both the smallest specific surface area of 1.07 m^2/g and largest mean particle size of 14.77 μm.

The morphologies of the MgO powders illustrated through observations gathered from the SEM images corresponded well with the particle characterization mentioned in Table 4. The surface structure of the MgH-650/1 particles provides an ample contact area for a rapid reaction. Therefore, it is expected that a MgO such as MgH-650/1 possessing a large surface area and low particle size, in combination with appropriate molar ratio formulation, should ultimately produce a MOC binder with the highest compressive strengths.

MOC Performance

Based on the aforementioned theory, because samples MgH-650/1 and MgH-850/1 have significantly higher surface areas compared with sample C-MgO, they are believed to be more reactive and thus have the potential to produce a MOC binder with a higher early strength.

The mixtures of produced MOC binder, made with different molar ratios of $MgO/MgCl_2$ and different variants of MgO, can be seen in Table 5. In the MOC sample name, the number following M denotes the molar ratio of $MgO/MgCl_2$ and the number following H denotes the molar ratio of $H_2O/MgCl_2$.

Flexural and Compressive Strengths of MOC Paste

The flexural strengths of the C-MgO, MgH-650/1, and MgH-850/1 samples are summarized in Fig. 5. The error bars for the flexural strength correspond to measured standard deviation in testing three prisms of each sample. The results show that as the molar ratio of $MgO/MgCl_2$ is increased, the flexural strength of the binder decreases. Sample MgH-650/1-M3H10 had the highest flexural strength of 38.6 MPa, whereas mixture C-MgO-M9H10 had the lowest flexural strength of 0.7 MPa. It was also found that a significant decrease of 19.0 MPa in flexural strength occurred for sample MgH-650/1 as the molar ratio of $MgO/MgCl_2$ increased from 3 to 5. However, ultimately, the highest flexural strength was still attained by sample MgH-650/1-M9H10 at 14.2 MPa. Moreover, as the molar ratio of $MgO/MgCl_2$ increased from 3 to 5 for samples C-MgO and MgH-850/1, the flexural strength exhibited only a small decrease of 2.5 and 0.9 MPa, respectively. However, for the same samples, a much more significant decrease in flexural strength takes place upon increasing the molar ratio of $MgO/MgCl_2$ from 5 to 9. This can be equated to an average reduction of 8.1 and 5.1 MPa per additional 2 moles of MgO for samples C-MgO and MgH-850/1, respectively.

As mentioned previously, evidence suggests that MgO samples MgH-650/1 and MgH-850/1 are more reactive than sample C-MgO and should therefore theoretically produce a MOC cement with a high early strength. This was found to be true throughout all molar ratios of $MgO/MgCl_2$. However, it was also found that samples with higher molar ratios of $MgO/MgCl_2$ exhibited more surface cracking, which would also inevitably result in a lower flexural strength because large defects such as cracks make the sample more susceptible to failure. The differences between cracking patterns in the MOC cement due to a varying molar ratio of $MgO/MgCl_2$ is demonstrated through the comparison of MOC samples C-MgO-M3H10 and C-MgO-M9H10 shown in Fig. 6. It is evident that the sample C-MgO-M9H10 has significant defects and cracks

Table 5. Molar composition of the blends and water to solids ratio (w/s)

Sample reference	Molar ratio		w/s
	$MgO/MgCl_2$	$H_2O/MgCl_2$	
C-MgO-M3/H10	3	10	0.22
C-MgO-M5/H10	5	10	0.179
C-MgO-M9/H10	9	10	0.179
MgH-650/1-M3/H10	3	10	0.22
MgH-650/1-M5/H10	5	10	0.178
MgH-650/1-M9/H10	9	10	0.344
MgH-850/1-M3/H10	3	10	0.22
MgH-850/1-M5/H10	5	10	0.178
MgH-850/1-M9/H10	9	10	0.251

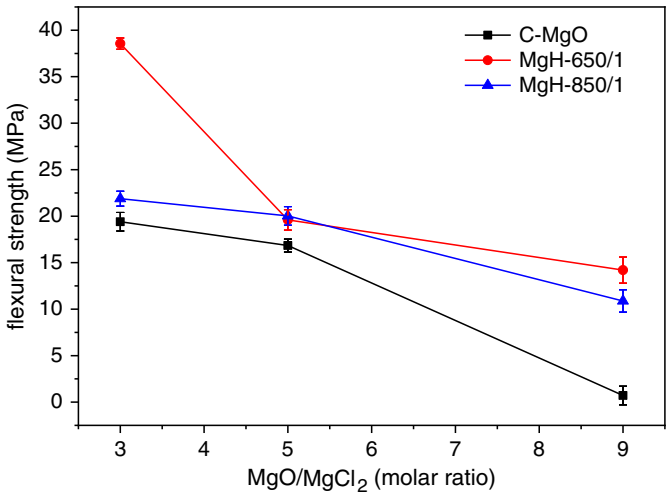

Fig. 5. Flexural strength of C-MgO, MgH-650/1, and MgH-850/1 after 7 days. Error bars correspond to measured standard deviation in testing three prisms of each sample.

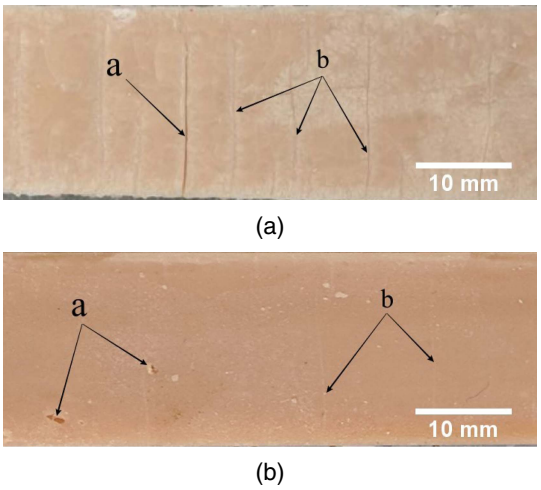

Fig. 6. Surface defects of (a) C-MgO-M9H10; and (b) C-MgO-M3H10.

[Points a and b in Fig. 6(a)], whereas C-MgO-M3H10 has only minor defects [Points a and b in Fig. 6(b)].

The compressive strengths of the C-MgO, MgH-650/1 and MgH-850/1 samples after 7 days of air curing are presented in Fig. 7. The error bars for the compressive strength correspond to measured standard deviation in testing three cubes of each sample. The results show that as the molar ratio of $MgO/MgCl_2$ was varied between 3 and 9, the compressive strengths of the C-MgO and MgH-650/1 samples increased. Sample MgH-650/1 attained the highest compressive strengths of 71.8, 93.0, and 111 MPa at molar ratios of 3, 5, and 9, respectively. However, the sample of MgH-850/1, although showing a dramatic increase in compressive strength with the transition of the $MgO/MgCl_2$ molar ratio from 3 to 5, exhibited a sharp fall in compressive strength at a molar ratio of 9. It is believed that the compressive strengths exhibited are the result of the particular phase assemblages produced, and the subsequent microstructure of the MOC binder. It is highly likely that the high specific surface area and thus reactivity of the MgO obtained from the calcination at 650 for 1 h, i.e., MgH-650/1, permitted for such high compressive strength to be obtained.

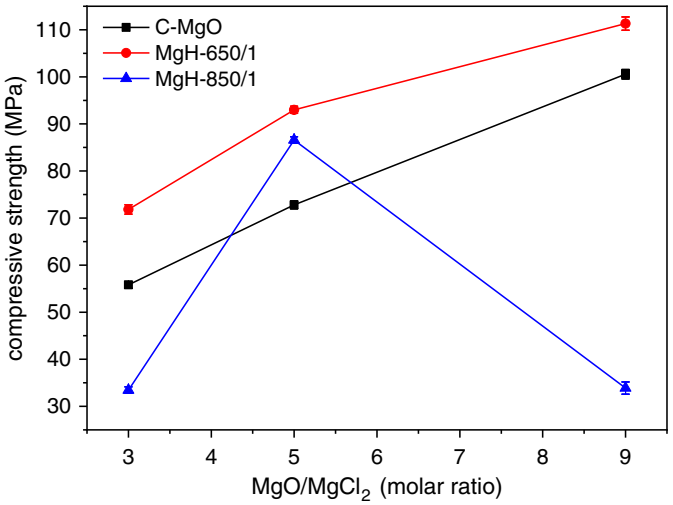

Fig. 7. Compressive strengths of C-MgO, MgH-650/1, and MgH-850/1 after 7 days. Error bars correspond to measured standard deviation in testing three cubes of each sample.

Moreover, it is thought that specimens with a higher compressive strength have a phase composition consisting dominantly of phase-5 hydration products, which is the most significant source of strength in the MOC system.

Phase Characterization

The influence of different MgO powder properties, namely the chemical composition (chemical purity), particle-size properties, and reactivity, on the microstructure was investigated and hence linked to the mechanical properties of MOC cement. The XRD spectra and SEM images of MOC mixtures formed from C-MgO are presented in Figs. 8 and 9, respectively. The XRD results illustrate that mixtures of C-MgO-M5H10 and C-MgO-M9H10 largely contain the favorable phase-5 reaction product. However, sample C-MgO-M9H10 had a much higher magnitude of unreacted MgO present than C-MgO-M5H10. This is due to C-MgO-M9H10 containing almost double the molar ratio of $MgO/MgCl_2$, leaving a significant amount of unconsumed MgO. Also, the mixture with the lowest $MgO/MgCl_2$ molar ratio of 3, i.e., C-MgO-M3H10, was detected to have the highest content of phase-3 crystals, fewer phase-5 crystals, and no unconsumed MgO.

The XRD spectra are shown to be in strong agreement with the acquired SEM images, which can be seen in Fig. 9. It can be observed from Fig. 9(a) that the mixture C-MgO-M3H10, consisted mostly of a homogenous distribution of phase-3 crystals without any unconsumed MgO. Fig. 9(b) of mixture C-MgO-M5H10 reveals that a significant amount of unconsumed MgO was detected. However, the denser microstructure also was observed to contain an abundance of phase-5 crystals appearing as scroll-tubular whiskers, explaining why the C-MgO-M5H10 sample produced a MOC binder with higher compressive strength than the C-MgO-M3H10 sample, namely because phase-5 crystals are known to be the primary contributors of mechanical strength (Chau and Li 2008b).

The XRD spectra and SEM images of MOC samples formed from MgH-850/1 are presented in Figs. 10 and 11, respectively. Again, the results show good agreement with each other, with the phase assemblages identified in the XRD, reflected accurately in the SEM images. Notably, it can be observed from the XRD spectra that a substantial content of $Mg(OH)_2$ is detected in the

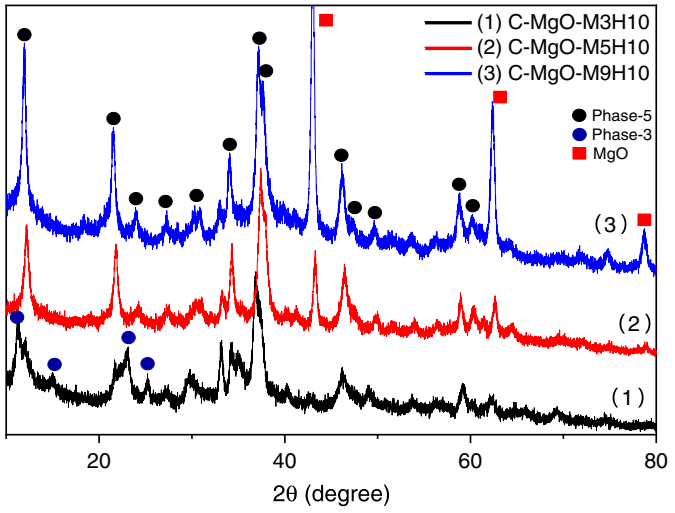

Fig. 8. XRD spectra of MOC samples made with commercial MgO (C-MgO).

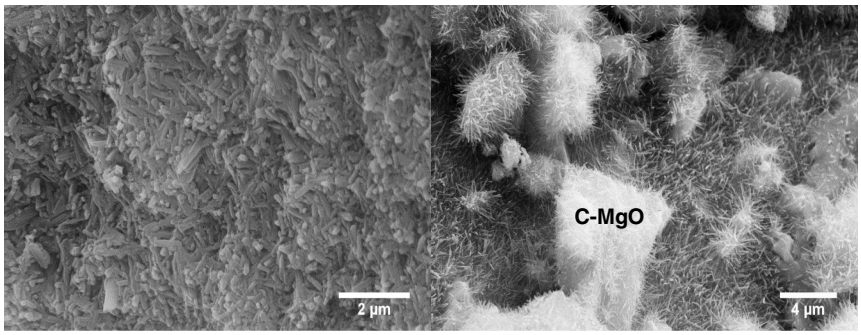

Fig. 9. SEM images of (a) C-MgO-M3H10; and (b) C-MgO-M5H10.

sample with the highest molar ratio of $MgO/MgCl_2$, i.e., MgH-850/1-M9H10. This is due to the large molar ratio of $H_2O/MgCl_2$ that was used (molar ratio of 10 + 2.78 moles of additional water to correct the workability of the paste).

In the SEM images in Fig. 11, sample MgH-850/1-M3H10 is observed to contain mostly phase-3 crystals [shown in Fig. 11(a)], which then go on to disappear with the increase of the $MgO/MgCl_2$ molar ratio from 3 to 5 and get replaced with phase-5 crystals, as shown in Fig. 11(b). Fig. 11(c) shows an abundant presence of sheet-like $Mg(OH)_2$ crystals and amorphous phase-5 crystals of a significantly less compact nature, appearing to be poorly formed with no evidence of intergrowth as observed in the MgH-850/1-M5H10 sample. The formation of $Mg(OH)_2$ is shown to be undesirable in the MOC system as the phase-5 intergrowth process is hindered and a less homogenous binder matrix is formed. The detection of the $Mg(OH)_2$ fits with the reduced compressive strength measured for the MgH-850/1-M9H10 sample presented in Fig. 7.

Furthermore, the XRD spectra and SEM images of MOC samples formed from MgH-650/1 using the $MgO/MgCl_2$ molar ratios of 3 and 5 are shown in Figs. 12 and 13, respectively. The XRD results reveal that unlike the MgH-850/1-M3H10 sample, which contained phase-3 crystals, for the equivalent molar ratio sample

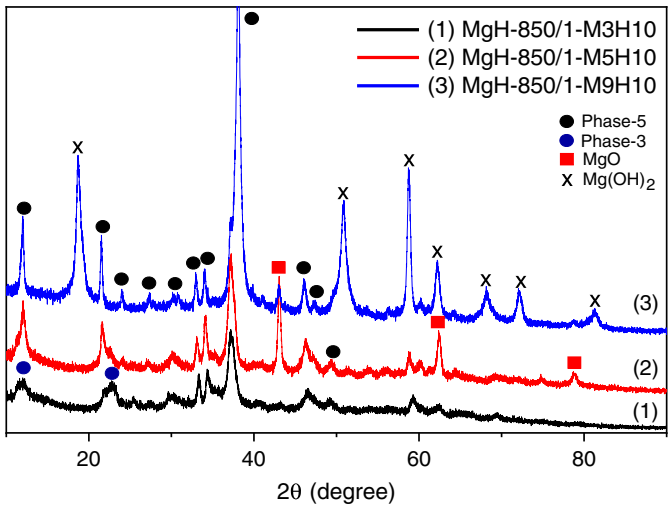

Fig. 10. XRD spectra of MOC samples made with MgH-850/1.

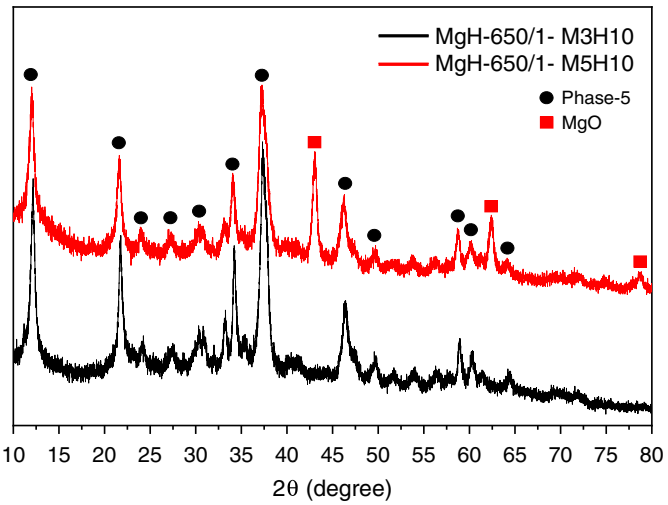

Fig. 12. XRD spectra of MOC samples made with MgH-650/1.

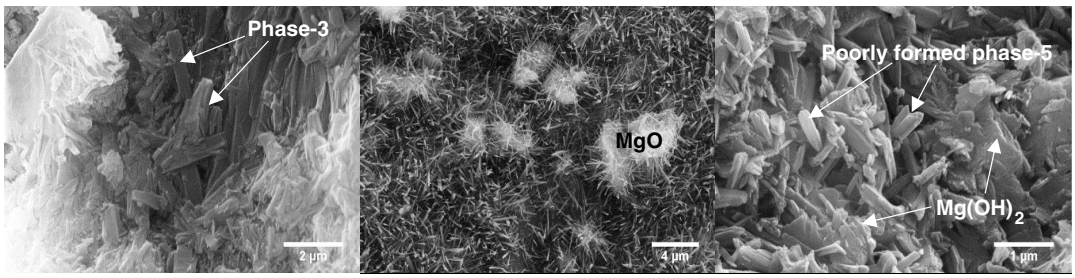

Fig. 11. SEM images of (a) MgH850-M3H10; (b) MgH850-M5H10; and (c) MgH850-M9H10.

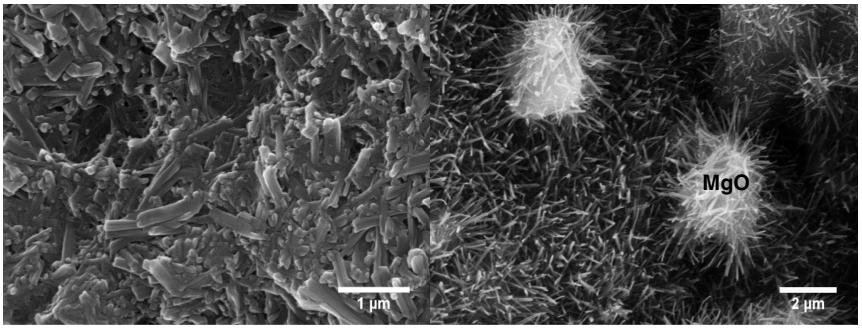

Fig. 13. SEM images of (a) MgH650-M3H10; and (b) MgH650-M5H10.

made with MgH-650/1, phase-3 crystals were not detected. Phase-5 crystals appeared to be the most prevalent in both MgH-850/1-M3H10 and MgH-850/1-M5H10 samples.

The SEM image in Fig. 13(a) reveals that the phase-5 crystals in sample MgH-850/1-M3H10, although still broken-tipped and interlocked, possess some characteristics of phase-3 crystals such as bulkiness and an irregular nature. It is understood that the transformation from phase-3 to phase-5 for a $Mg(OH)_2$ calcined at 650°C for 1 h occurs at the $MgO/MgCl_2$ molar ratio of 3, rather than 5 as is the case for the MgO calcined at 850°C. The microstructure observed in Fig. 13(b) of sample MgH-850/1-M5H10, however, followed the corresponding XRD results in Fig. 12, revealing a tightly packed microstructure of interlaced phase-5 crystals coexisting with unconsumed MgO particles. There is also an evident intergrowth mechanism of phase-5 crystals taking place within the microstructure that makes it more compact, corroborating the compressive strength results of sample MgH-650/1 presented in Fig. 7. The microstructure may also be described as largely homogeneous if the unconsumed MgO particles are disregarded; the neatly broken-tipped phase-5 crystals are in abundance throughout the entirety of the structure.

Conclusions

This study investigated the effects of varying calcination regimes on the chemical composition and morphology of formed MgO. The sustainability of $Mg(OH)_2$ compared with $MgCO_3$ was also examined. The influence of the molar ratio of $MgO/MgCl_2$ on the flexural and compressive strengths was also tested. Furthermore, a phase identification analysis of the produced MOC cement was conducted. The following significant conclusions may be drawn:

- The calcination temperature of $Mg(OH)_2$ is significantly more influential in controlling the chemical purity of the MgO than the duration of calcination. The reactivity of MgO was measured to be dependent on calcination temperature and in cases of higher temperature, on time too.
- WD-XRF and XRD results reveal that MgO acquired from the $Mg(OH)_2$ calcination duration of only 1 h can provide a significantly more superior quality MgO compared with $MgCO_3$ calcined at identical conditions.
- $Mg(OH)_2$ is a vastly superior precursor material for MOC than $MgCO_3$ due to its higher chemical purity and its sustainable calcination process. Namely, it allows for 17.6% lower energy consumption and 26.8% higher MgO yield.
- Higher calcination temperatures facilitate and cause MgO particles to agglomerate, consequently resulting in a larger mean particles size of MgO.
- The formation of $Mg(OH)_2$ was shown to be an undesirable hydration product in an MOC system with a $MgO/MgCl_2$ molar ratio of 5. $Mg(OH)_2$ posed a hindrance to the phase-5 intergrowth process, contributing to a less homogenous microstructure.

Acknowledgments

Financial support from the European Commission Horizon 2020 Research and Innovation Programme through Grant No. 723525 (i.e., Green INSTRUCT project) is greatly acknowledged.

References

Antonini, S., M. A. Arias, T. Eichert, and J. Clemens. 2012. "Greenhouse evaluation and environmental impact assessment of different urine-derived struvite fertilizers as phosphorus sources for plants." *Chemosphere* 89 (10): 1202–1210. https://doi.org/10.1016/j.chemosphere.2012.07.026.

Birchal, V. S., S. D. F. Rocha, M. B. Mansur, and V. S. T. Ciminelli. 2001. "A simplified mechanistic analysis of the hydration of magnesia." *Can. J. Chem. Eng.* 79 (4): 507–511. https://doi.org/10.1002/cjce.5450790406.

Chau, C. K., J. Chan, and Z. Li. 2009. "Influences of fly ash on magnesium oxychloride mortar." *Cem. Concr. Compos.* 31 (4): 250–254. https://doi.org/10.1016/j.cemconcomp.2009.02.011.

Chau, C. K., and Z. Li. 2008a. "Accelerated reactivity assessment of light burnt magnesium oxide." *J. Am. Ceram. Soc.* 91 (5): 1640–1645. https://doi.org/10.1111/j.1551-2916.2008.02330.x.

Chau, C. K., and Z. Li. 2008b. "Microstructures of magnesium oxychloride." *Mater. Struct.* 41 (5): 853–862. https://doi.org/10.1617/s11527-007-9289-y.

Chengyou, W., Z. Huifang, and Y. Hongfa. 2016. "Preparation and properties of modified magnesium oxysulfate cement derived from waste sulfuric acid." *Adv. Cem. Res.* 28 (3): 178–188. https://doi.org/10.1680/jadcr.15.00011.

Gu, J., Q. Zhang, J. Zhang, and W. Wang. 2010. "Studies on the preparation of polystyrene thermal conductivity composites." *Polym. Plast. Technol. Eng.* 49 (13): 1385–1389. https://doi.org/10.1080/03602559.2010.512326.

Li, C., and H. Yu. 2010. "Influence of fly ash and silica fume on water-resistant property of magnesium oxychloride cement." *J. Wuhan Univ. Technol.* 25 (4): 721–724. https://doi.org/10.1007/s11595-010-0079-y.

Li, Y., J. Sun, and B. Chen. 2014. "Experimental study of magnesia and M/P ratio influencing properties of magnesium phosphate cement." *Constr. Build. Mater.* 65: 177–183. https://doi.org/10.1016/j.conbuildmat.2014.04.136.

Li, Y., H. Yu, L. Zheng, J. Wen, C. Wu, and Y. Tan. 2013. "Compressive strength of fly ash magnesium oxychloride cement containing

granite wastes." *Constr. Build. Mater.* 38: 1–7. https://doi.org/10.1016/j.conbuildmat.2012.06.016.

Li, Z., and C. K. Chau. 2007. "Influence of molar ratios on properties of magnesium oxychloride cement." *Cem. Concr. Res.* 37 (6): 866–870. https://doi.org/10.1016/j.cemconres.2007.03.015.

Li, Z., and C. K. Chau. 2008. "Reactivity and function of magnesium oxide in sorel cement." *J. Mater. Civ. Eng.* 20 (3): 239–244. https://doi.org/10.1061/(ASCE)0899-1561(2008)20:3(239).

Liu, Z., S. Wang, J. Huang, Z. Wei, B. Guan, and J. Fang. 2015. "Experimental investigation on the properties and microstructure of magnesium oxychloride cement prepared with caustic magnesite and dolomite." *Constr. Build. Mater.* 85: 247–255. https://doi.org/10.1016/j.conbuildmat.2015.01.056.

Loganathan, P., G. Naidu, and S. Vigneswaran. 2017. "Mining valuable minerals from seawater: A critical review." *Environ. Sci.: Water Res. Technol.* 3 (1): 37–53.

Lu, Z., J. Zhang, G. Sun, B. Xu, Z. Li, and C. Gong. 2015. "Effects of the form-stable expanded perlite/paraffin composite on cement manufactured by extrusion technique." *Energy* 82: 43–53. https://doi.org/10.1016/j.energy.2014.12.043.

Marković, G., O. Veljković, M. Marinović-Cincović, V. Jovanović, S. Samaržija-Jovanović, and J. Budinski-Simendić. 2013. "Composites based on waste rubber powder and rubber blends: BR/CSM." *Compos. Part B Eng.* 45 (1): 178–184. https://doi.org/10.1016/j.compositesb.2012.08.013.

Misra, A. K., and R. Mathur. 2007. "Magnesium oxychloride cement concrete." *Bull. Mater. Sci.* 30 (3): 239–246. https://doi.org/10.1007/s12034-007-0043-4.

Purwajanti, S., L. Zhou, Y. Ahmad Nor, J. Zhang, H. Zhang, X. Huang, and C. Yu. 2015. "Synthesis of magnesium oxide hierarchical microspheres: A dual-functional material for water remediation." *ACS Appl. Mater. Interfaces* 7 (38): 21278–21286. https://doi.org/10.1021/acsami.5b05553.

Sadik, C., O. Moudden, A. El Bouari, and I. El Amrani. 2018. "Review on the elaboration and characterization of ceramics refractories based on magnesite and dolomite." *J. Asian Ceram. Soc.* 4 (3): 219–233. https://doi.org/10.1016/j.jascer.2016.06.006.

Sako, E. Y., M. A. L. Braulio, E. Zinngrebe, S. R. van der Laan, and V. C. Pandolfelli. 2012. "Fundamentals and applications on in situ spinel formation mechanisms in Al2O3-MgO refractory castables." *Ceram. Int.* 38 (3): 2243–2251. https://doi.org/10.1016/j.ceramint.2011.10.074.

Seeley, N. J. 2000. "Magnesian and dolomitic lime mortars in building conservation." *J. Archit. Conserv.* 6 (2): 21–29. https://doi.org/10.1080/13556207.2000.10785267.

Sglavo, V. M., F. De Genua, A. Conci, R. Ceccato, and R. Cavallini. 2011. "Influence of curing temperature on the evolution of magnesium oxychloride cement." *J. Mater. Sci.* 46 (20): 6726–6733. https://doi.org/10.1007/s10853-011-5628-z.

Walling, S. A., and J. L. Provis. 2016. "Magnesia-based cements: A journey of 150 years, and cements for the future?" *Chem. Rev.* 116 (7): 4170–4204. https://doi.org/10.1021/acs.chemrev.5b00463.

Yan, L. Y., X. F. Lu, Q. Guo, Q. H. Wang, and X. Y. Ji. 2014. "Research on the thermal decomposition and kinetics of byproducts from MgO wet flue gas desulfurization." *Adv. Powder Technol.* 25 (6): 1709–1714. https://doi.org/10.1016/j.apt.2014.06.018.

Zhou, X., and Z. Li. 2012. "Light-weight wood-magnesium oxychloride cement composite building products made by extrusion." *Constr. Build. Mater.* 27 (1): 382–389. https://doi.org/10.1016/j.conbuildmat.2011.07.033.

Zhu, J., N. Ye, W. Liu, and J. Yang. 2013. "Evaluation on hydration reactivity of reactive magnesium oxide prepared by calcining magnesite at lower temperatures." *Ind. Eng. Chem. Res.* 52 (19): 6430–6437. https://doi.org/10.1021/ie303361u.